Optimization of Shrinkage and Mechanical Properties in Continuous Glass Fiber-Reinforced Polypropylene Composite I-Beams during Pultrusion Process

Huihuang Ma[1,2], Zijian Wang[1], Yizhao Fu[1], Luo Luo[1] and Xiaodong Zhou[1,3,*]

[1]*Key Laboratory of Specially Functional Polymeric Materials and Related Technology (Ministry of Education), School of Chemical Engineering, East China University of Science and Technology, Shanghai, 200237, China*

[2]*Shanghai Key Laboratory of Multiphase Materials Chemical Engineering, School of Chemical Engineering, East China University of Science and Technology, Shanghai, 200237, China*

[3]*Institute for Engineering and Technology (Shanghai), Xinxing Cathay International Group, Shanghai, 400799, China*

Abstract: This study addresses shrinkage marks in pultruded continuous glass fiber-reinforced polypropylene I-beams by modifying the cooling mold with compensation segments, adding nano-SiO_2 as a nucleating agent, and incorporating glass fiber mesh. Under optimized conditions (80 mm/min, 235°C, 65–85–105°C), a compensation segment of 85 mm length and 0.5 mm depth effectively reduced surface shrinkage. Adding 2 wt% nano-SiO_2 lowered vertical shrinkage from 3.07% to 1.15% and horizontal shrinkage from 1.57% to 0.23%. An 8-mesh glass fiber grid further improved dimensional stability while maintaining a bending failure load of 5132.26 N and yield load of 3090 N. These strategies collectively enhance dimensional accuracy and mechanical performance in thermoplastic composite I-beams.

Keywords: Pultrusion process, Shrinkage marks, Nano-SiO_2, Glass fiber mesh, Composite I-beams.

1. INTRODUCTION

The pultrusion process of composite materials is primarily divided into two categories: thermosetting composite pultrusion and thermoplastic composite pultrusion. Thermosetting composites, having emerged earlier, have developed more mature molding processes. Extensive research has been conducted on the pultrusion process for thermosetting composites, including investigations into the molds, fiber content, fiber diameter, and filler amounts [1, 2]. Simultaneously, modeling and simulation studies of the curing process during the molding of thermosetting composites have been ongoing [3, 4].

Despite extensive studies on the pultrusion and curing processes of thermosetting composites, thermosetting resins are inherently limited by their physical properties, which prevent recycling and reuse. This limitation makes thermosetting resins unsuitable for sustainable development, leading to a market shift toward thermoplastic composites. Thermoplastic composites are increasingly favored due to their superior mechanical properties, good heat resistance, corrosion resistance, electrical properties, high production efficiency, and ease of recycling. These advantages have made thermoplastic composites one of the most widely applied materials. Compared to other composite molding processes, the thermoplastic pultrusion process offers low cost, high efficiency, and high utilization rates.

However, a key challenge in thermoplastic pultrusion is the effective impregnation of fiber reinforcements due to the high melt viscosity of the resin matrix. Consequently, pre-impregnation is typically required, and the quality of impregnation critically influences the final product's properties [5-7].

Significant research efforts have therefore focused on modeling impregnation [6, 8], optimizing impregnation parameters [5, 7, 9], and understanding the mechanical behavior of thermoplastic composites [10, 11]. Process parameter studies, such as the role of pultrusion speed and temperature[12], and the development of novel reactive pultrusion systems [13], have also been conducted.

While many scholars focus on the performance of thermoplastic composites and the impregnation of fibers by resins, there has been limited research on the thermoplastic composite pultrusion process itself. Moreover, pultrusion of thermoplastic composites generally produces rod-shaped products, leading to a lack of reference for pultruding non-rod shapes, making it difficult to determine reasonable feed rates and process parameters. This gap is particularly evident in the manufacturing of I-beams.

*Address correspondence to this author at the Key Laboratory of Specially Functional Polymeric Materials and Related Technology (Ministry of Education), School of Chemical Engineering, East China University of Science and Technology, Shanghai, 200237, China; E-mail: xdzhouecust@126.com

Received on 02-11-2025 Accepted on 08-12-2025 Published on 15-12-2025

E-ISSN: 2311-8717/25

In the case of I-beams, research has mostly been limited to the use of steel or wooden I-beams in various applications [14-17], with substantial room for exploration regarding the materials used. Li [18] developed thermosetting composite I-beams with different performance levels to meet the requirements of varying voltage levels and established product standards for composite I-beams used in ultra-high voltage converter valves. Zhang [19] conducted finite element simulations of GFRP I-beams, focusing on the effect of fiber placement angle in the web on shear stress. Yi [20] investigated the bending performance of three-dimensional five-directional woven composite I-beams, finding that the weaving angle and fiber volume fraction were key performance factors. Lacki [21] studied the impact of glass fiber-reinforced polyurethane foam on the bending performance of three types of I-beams. Hai [22] researched the structural performance of hybrid fiber-reinforced polymer beams, optimizing the use of carbon and glass fibers and reducing overall costs while maximizing structural performance. They also found that the flange-to-web width ratio of the I-beam plays a crucial role in its structural behavior.

In the pultrusion process of continuous glass fiber-reinforced polypropylene thermoplastic composite I-beams, shrinkage occurs when the I-beam exits the cooling mold due to the crystallization, orientation, and cooling of the resin. This shrinkage is most noticeable in the web, where a prominent shrinkage mark forms at the center of the web (as shown in Figure **1**), significantly affecting the appearance of the pultruded I-beam. Additionally, the shrinkage marks induce stress concentration, making the I-beam more prone to failure under load.

Therefore, this study aims to address this research gap by systematically investigating the formation mechanism of shrinkage marks in pultruded GF/PP I-beams and developing practical solutions. The results are analyzed, and the feasibility and practicality of the proposed solutions are discussed. The novelty of this work lies in the integrated approach addressing shrinkage in pultruded thermoplastic I-beams, which includes: (1) the design of a compensated cooling mold channel to offset volumetric shrinkage geometrically; (2) the inter-layer application of nano-SiO_2 as a nucleating agent between prepregs to modify crystallization behavior; and (3) the use of glass fiber mesh as a supporting reinforcement to mitigate shrinkage stress and enhance mechanical performance simultaneously.

2. THEORETICAL ANALYSIS AND EXPERIMENTAL

2.1. Mechanism of Shrinkage Mark Formation

The formation of shrinkage marks on the I-beam can be attributed to the relatively thick and wide web. During cooling and crystallization, the polypropylene resin contracts. Because the inner edges of the flanges are constrained by the cooling mold (preventing inward displacement), the resultant tensile stresses within the resin become concentrated at the geometric center of the web's top and bottom surfaces. Consequently, the force concentrates at the central point of the top and bottom surfaces of the I-beam, as illustrated in Figure **2**, leading to the formation of shrinkage marks.

The primary drivers of resin shrinkage are (1) thermal contraction upon cooling, (2) volumetric reduction due to crystallization, and (3) relaxation of molecular orientation. These effects are interdependent but can be analyzed separately to understand their contributions.

Cooling shrinkage occurs because the resin matrix expands upon heating. The extent of shrinkage is directly related to the thermal expansion coefficient. The shrinkage of the resin product is the difference between the expansion of the resin at high

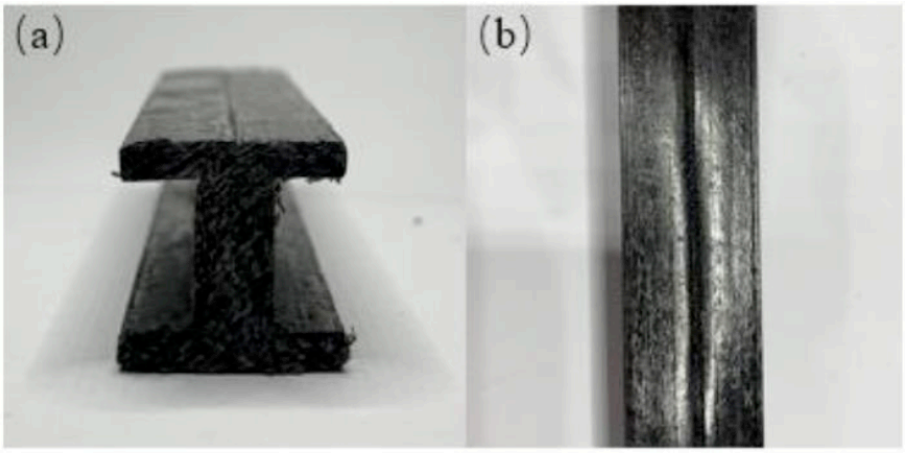

Figure 1: I-beam web contraction pattern (**a**) front view (**b**) top view.

temperatures and that of the mold material. During processing, the molding temperature of the product is close to the mold temperature; however, the coefficient of linear thermal expansion of the mold material is significantly lower than that of the resin material. Therefore, as the temperature increases, the expansion of the resin material greatly exceeds that of the mold material, resulting in an increase in product shrinkage.

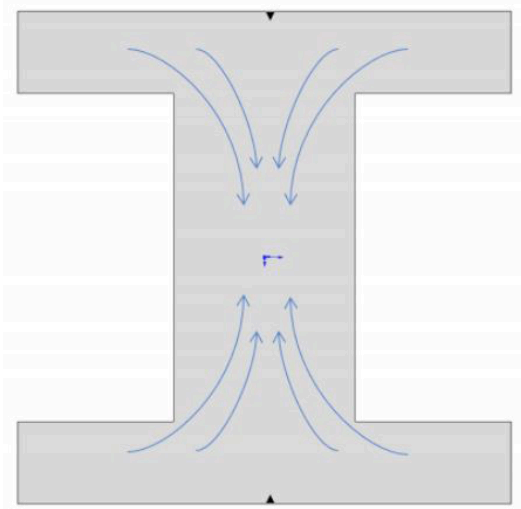

Figure 2: Shrinkage stress of I-beam.

The specific degree of shrinkage can be calculated using Equation 1.

$$\Delta H = H_0[\alpha_r(T_r - T_0) - \alpha_m(T_m - T_0)] \quad (1)$$

Herein, ΔH represents the shrinkage of the resin product, H_o refers to the dimensions of the resin product at room temperature, α_r is the coefficient of linear thermal expansion of the resin, T_r is the molding temperature of the resin, T_o is the room temperature (20°C), α_m is the coefficient of linear thermal expansion of the mold material, and T□ is the mold temperature. Critically, because $\alpha_r >> \alpha_m$, the resin contracts significantly more than the mold upon cooling from T_r to T□, resulting in the net shrinkage ΔH. A higher molding temperature (T_r) directly leads to greater thermal shrinkage. The equation indicates that the higher the molding temperature, the greater the shrinkage of the resin product.

Orientation refers to the phenomenon where polymer molecular chains and crystallites preferentially align in the direction of an applied external force. This phenomenon occurs only under the influence of an external force. Both orientation and crystallization are products of the ordered arrangement of polymer molecular chains; however, they differ in that crystallization involves three-dimensional order, while orientation involves one-dimensional or two-dimensional order. The pultrusion process is one that involves stretching along a single direction. During this process, the resin molecular chains inevitably align parallel to the direction of the applied force, leading to uniaxial orientation. The strength of this orientation is influenced by both temperature and stretching. As the resin temperature decreases, the resin undergoes cooling, and the exterior of the product is shaped. During this process, the internal stretching forces weaken, and the molecular chains inside the product tend to revert to their original state, leading to the de-orientation process. This results in shrinkage in the orientation direction of the I-beam. The degree of polymer orientation can be expressed using Equation 2.

$$F = \frac{3\cos^2\theta - 1}{2} \quad (2)$$

Here, F represents the degree of orientation, and θ is the angle between the main axis of the molecular chain and the orientation direction. During cooling, as the tensile force exerted by the process diminishes, these oriented chains tend to relax toward a more random coil state (de-orientation). This recovery process manifests as additional shrinkage along the pultrusion axis and can cause slight compensatory expansion in the transverse directions.

In summary, the total shrinkage observed in the I-beam web is the combined result of these three mechanisms. The stress concentration arising from this constrained volumetric change, particularly in the thick web, is the direct cause of the visible surface shrinkage mark.

2.2. Experimental Study on Shrinkage Mark Improvement

Cooling shrinkage is an inherent property of materials, and it is challenging to alter its magnitude without modifications at the microscopic level. Therefore, this work focus on addressing the issue from a processing perspective. By modifying the channel in the original cooling mold, compensation for the shrinkage is provided to alleviate the formation of shrinkage marks. The mold channel corresponding to the shrinkage marks on the I-beam is polished using abrasive tools to create a tapered shape. Additionally, a flat region is left at the exit of the cooling mold to ensure the final product's surface remains smooth. The shrinkage of the resin is calculated using Equation 1, where the thermal expansion coefficient of continuous glass fiber-reinforced polypropylene is taken as 9.05×10^{-5} K^{-1}, and that of the mold material is 12.9×10^{-6} K^{-1}. Based on these values, the shrinkage amount is calculated, and the cooling mold channels are modified accordingly. The effect of compensation segment

length on the shrinkage marks of the I-beam is then studied. Since the cooling and shaping of the I-beam are also influenced by the pultrusion speed and the temperature gradient of the cooling mold, the study of the compensation segment requires first determining the processing conditions for the pultrusion process. The optimal conditions for the I-beam performance are adopted, with the pultrusion speed set to 80 mm/min, the mold temperature set to 235°C, and the cooling mold temperature gradient set to 65-85-105°C.

2.3. Experimental Study on Shrinkage Rate Improvement

To address the shrinkage marks on the I-beam surface caused by crystallization, this experiment aims to reduce the crystallinity of the polypropylene resin, resulting in a more disordered crystalline arrangement. Since continuous glass fiber-reinforced polypropylene prepreg has been pre-prepared and is used as the raw material for the pultrusion process, it is not possible to modify the crystallization process through grafting polypropylene or adding nucleating agents. However, the crystallization structure between the prepreg layers can be altered to reduce shrinkage. Polypropylene, being a non-polar substance, does not dissolve in anhydrous ethanol. Furthermore, as polypropylene consists of saturated carbon chains, it does not react with alcohols or acids, and anhydrous ethanol can spread on the surface of polypropylene. In this experiment, a homogenizer is used to disperse nano-SiO_2 evenly in anhydrous ethanol, which is then applied to the surface of the prepreg. The prepreg is then directly fed into the pultrusion mold. The ethanol on the surface of the prepreg rapidly vaporizes at the high temperature inside the mold, and under the pressure from the mold, the ethanol is expelled from the composite material. The nano-SiO_2 particles, however, are trapped by the molten resin matrix and uniformly arranged between the prepreg layers. During cooling and crystallization, the nano-SiO_2 acts as a nucleating agent, promoting the formation of additional crystalline grains. This results in a reduction of the molecular chain regularity and a decrease in the shrinkage rate.

3. RESULTS AND DISCUSSION

3.1. Analysis of Shrinkage Phenomenon in I-Beams

The vertical and horizontal dimensions of the I-beam are shown in Figure **3**, with corresponding labels for each part's dimensions. Here, a represents the height of the I-beam, b represents the thickness of the web, and c represents the flange width. The actual shrinkage rate of the composite material I-beam can be calculated using Equation 3.

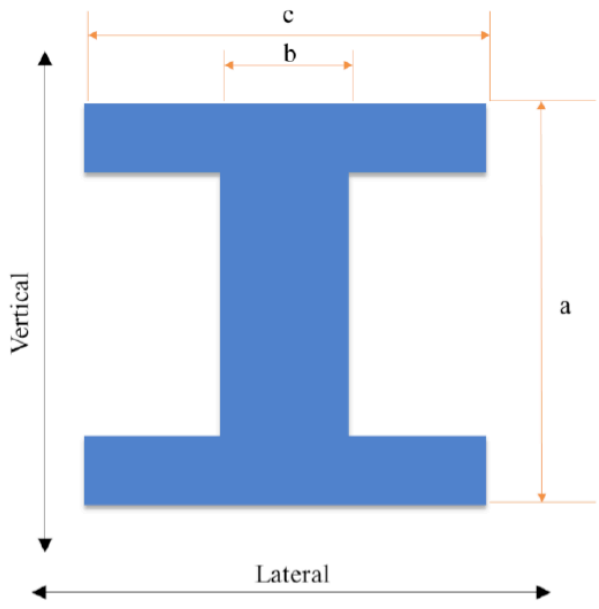

Figure 3: I-beam direction and size symbol.

$$S = \frac{L_0 - L_r}{L_0} \times 100\% \quad (3)$$

Where S is the shrinkage rate, L_0 is the theoretical dimension of the I-beam, and L_r is the actual dimension of the fabricated I-beam.

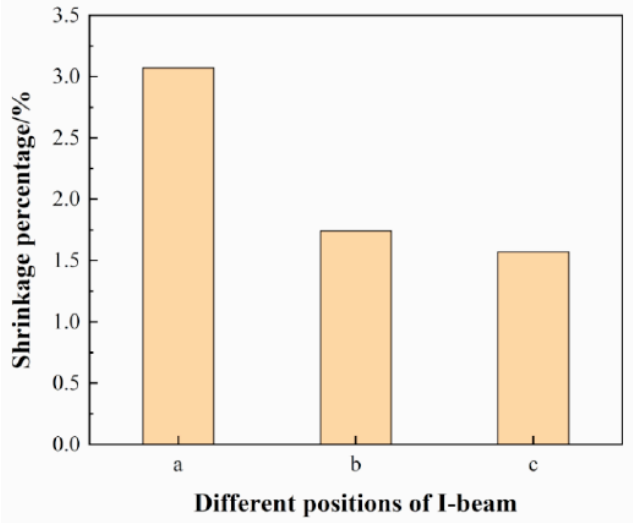

Figure 4: The shrinkage rate of each part of the I-beam.

The shrinkage rates at various positions of the actual I-beam are measured and shown in Figure **4**. The shrinkage rate at position a is 2.62%, at position b it is 0.63%, and at position c it is 0.58%. It is evident that the transverse shrinkage rate is relatively low in the I-beam, which is primarily due to the thin flange. The thinness results in less resin content at the flange, while the larger contact area with the cooling mold (and hence greater heat exchange area) allows the flange to cool more quickly. This rapid cooling facilitates the formation of more crystalline nuclei during resin cooling

and crystallization, resulting in finer crystalline grains and more disorder in their arrangement, which mitigates crystallization shrinkage. On the other hand, the transverse shrinkage at the web is smaller because, during the pultrusion process, the molecular chains of polypropylene resin undergo orientation. As cooling and shaping take place, the resin in the web cools more slowly, leading to a phenomenon of de-orientation within the molecular chains. This causes axial shrinkage in the pultrusion direction and some radial expansion, partially offsetting the shrinkage caused by crystallization and cooling. In the vertical direction, however, due to the longer length, the impact of cooling and crystallization shrinkage is much greater than that of orientation shrinkage. The expansion provided by de-orientation in the vertical direction cannot counteract the effects of the other two factors, resulting in a significantly higher vertical shrinkage rate compared to the transverse shrinkage rate.

3.2. Effect of Mold Flow Channel Treatment on Shrinkage Marks

Since the shrinkage of the I-beam during the pultrusion process is a continuous dynamic phenomenon, the shrinkage increases as the I-beam advances through the cooling mold. Upon entering the cooling mold, the temperature change is significant and exceeds the crystallization temperature, so cooling shrinkage dominates, and its magnitude can be calculated using Equation 1. As the temperature gradually changes according to the mold temperature gradient, the rate of temperature change decreases, and it eventually drops to the crystallization temperature, at which point crystallization shrinkage takes precedence. Therefore, the dimensions of the compensation section in the cooling mold's flow channel have a significant impact on the appearance of the composite I-beam. Figure **5** shows the appearance of I-beam samples under different compensation section conditions. In Figure **5a**, the middle portion exhibits a protrusion, indicating sufficient compensation at the center but insufficient compensation on the sides, failing to completely offset the cooling shrinkage. In Figure **5b**, shrinkage marks are still present, which is due to the insufficient length of the compensation section, which only compensates for the cooling shrinkage but does not adequately address the crystallization shrinkage. Through continuous improvement of the compensation section, the final I-beam (shown in Figure **5d**) is obtained, where the compensation section has a length of 85 mm, a depth of 0.5 mm, and a rounded cross-sectional shape.

3.3. Effect of Nano-SiO_2 on Shrinkage of I-Beams

First, the mass per unit length of the composite I-beam is calculated using Equation 4:

$$m = \rho \times S \tag{4}$$

Where m is the mass per unit length of the composite I-beam (g/cm), ρ is the density of the composite I-beam, and S is the cross-sectional area of the composite I-beam. This standard allows the determination of the mass content of nano-SiO_2 in the I-beam products. In this experiment, nano-SiO_2 is added to the prepreg layers during the pultrusion process. It does not fully

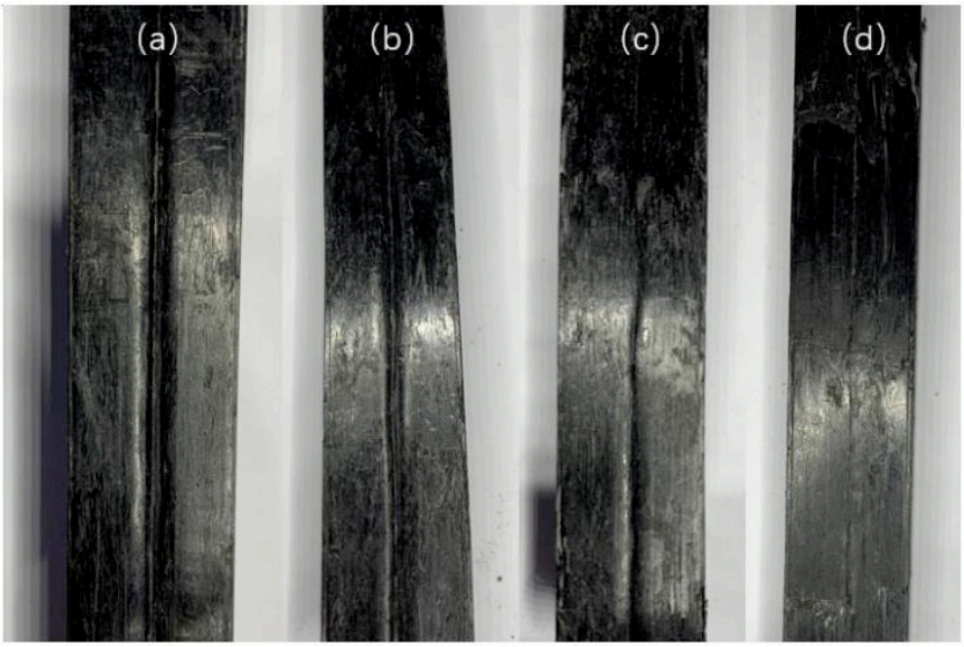

Figure 5: Variation of shrinkage lines of I-beam under different compensation section lengths.

mix with the polypropylene resin but is instead applied as a coating between the layers of the prepreg, altering the crystallization structure between the layers.

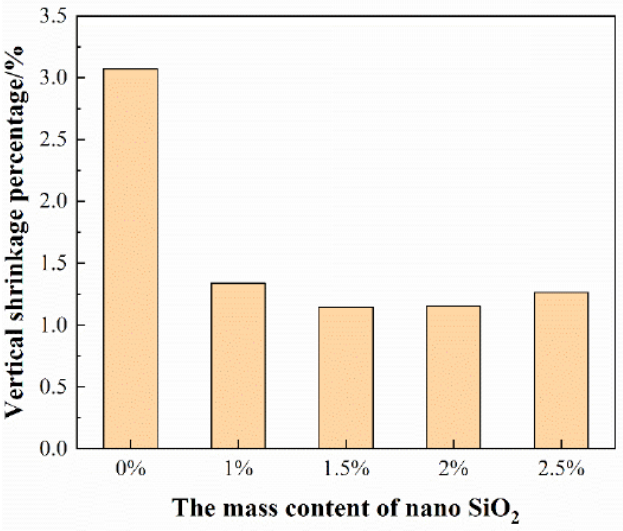

Figure 6: The influence of nano-SiO_2 content on the vertical shrinkage of I-beam.

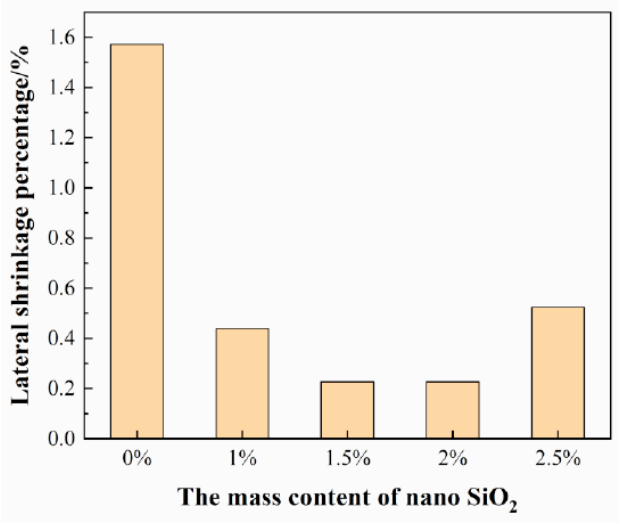

Figure 7: The influence of nano-SiO_2 content on the lateral shrinkage of I-beam.

As shown in Figures **6** and **7**, when a small amount of nano-SiO_2 is added between the prepreg layers, both the vertical and horizontal shrinkage of the I-beam are significantly improved. At low concentrations (*e.g.*, ≤2 wt%), the well-dispersed nano-SiO_2 particles act as effective nucleating agents. This promotes the formation of a larger number of smaller spherulites during polypropylene crystallization. This refined crystalline structure, with its reduced spherulite size and increased inter-crystalline boundaries, creates a more compliant microstructure that better accommodates shrinkage stresses, thereby diminishing overall volumetric contraction. Furthermore, the particles at the interlayer may slightly hinder polymer chain packing, contributing to a modest reduction in overall crystallinity, which directly mitigates crystallization shrinkage.

However, as the amount of nano-SiO_2 increases, its impact on the shrinkage of the composite I-beam begins to diminish. When the mass content reaches 2.5%, the shrinkage rate of the I-beam even increases. This is attributed to two concurrent factors at high filler loading: First, nanoparticle aggregation becomes prevalent. These aggregates act as macroscopic defects and stress concentrators, disrupting the uniformity of the microstructure and creating pathways for localized shrinkage. Second, despite the potential for aggregation, the exceedingly high number of nucleation sites can paradoxically lead to an overall increase in the degree of crystallinity. Since the crystallization process itself is densification, a higher final crystallinity results in greater crystallization shrinkage. At high nano-SiO_2 content, this strong shrinkage-driving force, compounded by the defects from aggregation, overcomes the shrinkage-reducing benefit of crystal refinement, leading to a net increase in shrinkage rate.

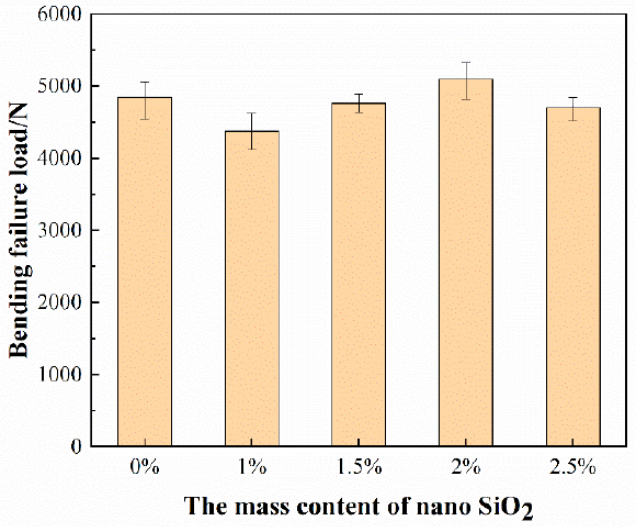

Figure 8: The influence of nano-SiO_2 content on the bending performance of I-beam.

The experiment also investigates the effect of nano-SiO_2 on the mechanical properties of the composite I-beam. As shown in Figure **8**, when nano-SiO_2 is first added, the mechanical properties of the composite I-beam decrease significantly. This is because a low, non-uniform distribution of nano-SiO_2 can create localized stress fields and weak interfacial regions between the prepreg layers, initiating microcracks that facilitate premature failure under load. However, as the nano-SiO_2 content increases to an optimal level (around 2%), the mechanical properties improve. At this optimal concentration, a more uniform particle distribution is achieved. This uniformity ensures a homogeneous refinement of the crystalline

morphology throughout the interlayer regions. The multitude of fine spherulites and the strong interfacial adhesion, when nanoparticles are well-dispersed, enhance load transfer and toughness. The refined microstructure can more effectively deflect and arrest growing cracks, thereby improving bending performance. Beyond this optimum, when the content reaches 2.5%, the mechanical properties decline again. This is due to severe nanoparticle aggregation. These aggregates form large, weak interfaces and internal voids, which become primary sites for crack initiation and propagation under stress, significantly compromising the structural integrity and leading to reduced failure loads.

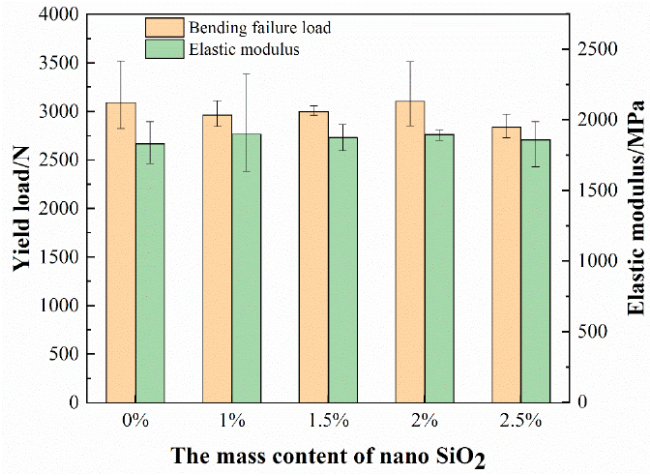

Figure 9: The influence of SiO_2 content on the yield of I-beam.

Figure **9** demonstrates the trend in the yield capacity of the composite I-beam as the mass content of nano-SiO_2 changes. Initially, the yield load decreases. This initial drop is consistent with the introduction of stress-concentrating inhomogeneities at very low filler content. As the nano-SiO_2 content increases to the optimum, the yield load recovers and improves. This recovery is driven by the aforementioned benefits of a homogeneously refined crystalline structure and enhanced interlayer bonding, which strengthen the material against yielding. Finally, at 2.5% content, the yield strength decreases again, directly resulting from the catastrophic effect of particle aggregates acting as large-scale defects that promote yielding at lower stresses.

3.4. Effect of Glass Fiber Mesh on Shrinkage of I-Beam Products

As shown in Figure **10**, the addition of mesh fabric improves the vertical and horizontal shrinkage marks of the I-beam. The mesh fabric functions through a dual mechanism: first, as a heterogeneous nucleating agent, it promotes the formation of finer polypropylene spherulites, which reduces crystallization shrinkage; second, its integrated fibrous structure provides direct mechanical restraint against the tensile stresses generated during cooling and crystallization, thereby counteracting shrinkage deformation.

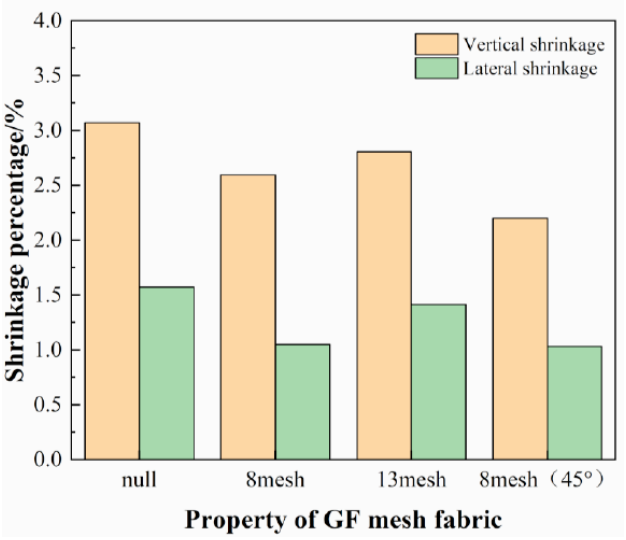

Figure 10: The influence of grid cloth on the shrinkage rate of I-beam.

A clear comparison of the three mesh types reveals their distinct effectiveness. The 45° twill fabric yielded the greatest shrinkage reduction (28.36% vertical, 34.43% horizontal), attributed to its off-axis filaments which most effectively disrupt the anisotropic flow and shrinkage patterns. The 8-mesh fabric also provided substantial improvement (15.49% vertical, 33.33% horizontal), offering a balanced combination of open structure for resin penetration and sufficient reinforcement. The 13-mesh fabric, while beneficial, showed more modest gains (8.61% vertical, 10.07% horizontal), likely due to its tighter weave which may limit optimal resin permeation and interfacial bonding in this process.

This mechanical reinforcement directly contributes to the observed shrinkage reduction. This improvement is due to the fact that the glass fiber mesh is added to both the flange and the web of the I-beam, where it acts as a heterogeneous nucleating agent for polypropylene resin, facilitating the formation of smaller crystals during crystallization. Additionally, the mesh fabric provides support, counteracting the stresses induced by crystallization and cooling shrinkage, thus reducing the shrinkage rate. The best performance is achieved with the 45° twill mesh fabric, as its asymmetric weave geometry provides multi-axial constraint and most effectively impedes the propagation of shrinkage-related stress through the composite cross-section.

4. CONCLUSION

This study presents several distinct contributions to the pultrusion of thermoplastic composite profiles:

firstly, a novel compensation-segment design within the cooling mold effectively reduces surface shrinkage marks; secondly, a method of applying nano-SiO_2 between prepreg layers is introduced to control crystallization shrinkage without full resin blending; thirdly, glass fiber mesh is employed as an integrated reinforcement, improving both dimensional stability and load-bearing capacity.

(1) A novelly designed compensation segment within the cooling mold was proven effective in eliminating surface shrinkage marks. Under optimized process conditions (pultrusion speed: 80 mm/min; mold temperature: 235°C; cooling gradient: 65–85–105°C), a segment with a length of 85 mm, a depth of 0.5 mm, and a rounded profile provided optimal geometric compensation for the combined thermal and crystallization shrinkage.

(2) The inter-layer application of nano-SiO_2 as a coating between prepregs significantly refined the crystalline structure. At an optimal mass content of 2%, it reduced the vertical shrinkage rate from 3.07% to 1.15% and the horizontal shrinkage rate from 1.57% to 0.23%. This method offers a practical route to control crystallization-induced shrinkage without compromising processability.

(3) Incorporating glass fiber mesh provided dual benefits of mechanical reinforcement and shrinkage restraint. While the 45° twill mesh yielded the greatest shrinkage reduction (vertical: -28.26%; horizontal: -34.43%), the 8-mesh fabric presented the best overall compromise, delivering a bending failure load of 5132.26 N and a yield load of 3090 N, while still reducing vertical and horizontal shrinkage rates by 15.49% and 33.33%, respectively.

Collectively, these strategies demonstrate a viable pathway for manufacturing high-quality thermoplastic composite I-beams with improved dimensional accuracy (target shrinkage rates below 2.6% vertically and 1.1% horizontally) and enhanced mechanical performance, which is directly relevant to industrial applications requiring lightweight, recyclable structural profiles. A limitation of this work is the focus on a specific polypropylene/glass fiber system and I-beam geometry; future work will explore the transferability of these methods to other thermoplastic matrices and more complex profile shapes, as well as long-term environmental durability assessments.

CONFLICTS OF INTEREST

The authors declare that they have no known competing financial interests or personal relationships that could have appeared to influence the work reported in this paper.

REFERENCE

[1] Strauß S, Wilhelm F. Development of a Flexible Injection and Impregnation Chamber for Pultrusion of High Reactive Resins. Procedia Manufacturing 2020; 47: 956-61. https://doi.org/10.1016/j.promfg.2020.04.294

[2] Tucci F, Esperto V, Rubino F, Carlone P. Experimental Measurement of the Resistant Load in Injection Pultrusion Processes. Procedia Manufacturing 2020; 47: 148-53. https://doi.org/10.1016/j.promfg.2020.04.157

[3] Nasonov Y, Safonov A, Gusev S, Akhatov I. Effect of Additives on Cure Kinetics of Pultrusion Resins. Procedia Manufacturing 2020; 47: 920-4. https://doi.org/10.1016/j.promfg.2020.04.283

[4] Barkanov E, Akishin P, Miazza NL, Galvez S, Pantelelis N. Experimental validation of thermo-chemical algorithm for a simulation of pultrusion processes. J Phys: Conf Ser 2018; 991: 012009. https://doi.org/10.1088/1742-6596/991/1/012009

[5] Studer J, Dransfeld C, Jauregui Cano J, Keller A, Wink M, Masania K, *et al*. Effect of fabric architecture, compaction and permeability on through thickness thermoplastic melt impregnation. Composites Part A: Applied Science and Manufacturing 2019; 122: 45-53. https://doi.org/10.1016/j.compositesa.2019.04.008

[6] Man Y, Yadong H, Rui L, *et al*. Melt Impregnation Model of Continuous Fiber Reinforced Thermoplastic Composites. Plastics Science and Technology 2019,47(07): 12-17.

[7] Hopmann C, Wilms E, Beste C, Schneider D, Fischer K, Stender S. Investigation of the influence of melt-impregnation parameters on the morphology of thermoplastic UD-tapes and a method for quantifying the same. Journal of Thermoplastic Composite Materials 2021; 34: 1299-312. https://doi.org/10.1177/0892705719864624

[8] Deng T, Zhang W, Jiang W, Zhou H, Huang Z, Peng X, *et al*. A hybrid lamination model for simulation of woven fabric reinforced thermoplastic composites solid-state thermo-stamping. Materials & Design 2021; 200: 109419. https://doi.org/10.1016/j.matdes.2020.109419

[9] Shan H, Li M, Guo BB, Zhou XD, Zheng Q, Chen CJ. Influence of process conditions on the mechanical properties of powder-impregnated CF/PEEK prepreg laminates. Aerosp Shanghai 2019; 36: 127-134.

[10] Cui J, Wang S, Wang S, Li G, Wang P, Liang C. The Effects of Strain Rates on Mechanical Properties and Failure Behavior of Long Glass Fiber Reinforced Thermoplastic Composites. Polymers 2019; 11: 2019. https://doi.org/10.3390/polym11122019

[11] Singh AK, Siddhartha. An investigation on the mechanical and thermal performance of a novel functionally graded materials-based thermoplastic composites. Journal of Thermoplastic Composite Materials 2019; 32: 1691-713. https://doi.org/10.1177/0892705718805124

[12] Jing R, Zhang RT, Meng YC, Wang YH, Zhang XG, Zhao Y, Zhang YB. Process parameters in pultrusion of continuous glass fiber/polypropylene thermoplastic composites. Acta Mater Compos Sin 2020; 37: 2782-2788.

[13] Chen K, Jia M, Hua S, Xue P. Optimization of initiator and activator for reactive thermoplastic pultrusion. J Polym Res 2019; 26: 40. https://doi.org/10.1007/s10965-019-1708-6

[14] Zheng CH, Zhou GM, Dong WF, Wang Y, Cao R. Study on bending performance of 3D five-directional braided composite I-beam. Fiber Glass 2014; 39-45.

[15] Asl ME, Niezrecki C, Sherwood J, Avitabile P. Similitude Analysis of Composite I-Beams with Application to Subcomponent Testing of Wind Turbine Blades. Experimental and Applied Mechanics, Volume 4. 1st ed., New York: River Publishers; 2025, p. 115-26. https://doi.org/10.1007/978-3-319-22449-7_14

[16] Goswami R, Murty CVR. Externally Reinforced Welded I-Beam-to-Box-Column Seismic Connection. J Eng Mech 2010; 136: 23-30. https://doi.org/10.1061/(ASCE)0733-9399(2010)136:1(23)

[17] Rudakov IA. Problem on Periodic Vibrations of an I-beamwith Clamped Endpoint in the Resonance Case. Diff Equat 2020; 56: 330-9. https://doi.org/10.1134/S0012266120030064

[18] Li DX. Research on high-performance glass fiber reinforced composite I-beam. Southwest Univ Sci Technol 2019.

[19] Zhang S. Study on mechanical properties of GFRP and concrete composite beam with grid. Harbin Eng Univ 2017.

[20] Yi QS, Zhong YF, Peng X. Reconstruction of three-dimensional local fields in FRP laminated I-beam based on variational asymptotic method. Proc 29th Natl Conf Struct Eng 2020; 219-222.

[21] Lacki P, Derlatka A, Winowiecka J. Analysis of the composite I-beam reinforced with PU foam with the addition of chopped glass fiber. Composite Structures 2019; 218: 60-70. https://doi.org/10.1016/j.compstruct.2019.03.036

[22] Hai ND, Mutsuyoshi H, Asamoto S, Matsui T. Structural behavior of hybrid FRP composite I-beam. Construction and Building Materials 2010; 24: 956-69. https://doi.org/10.1016/j.conbuildmat.2009.11.022

https://doi.org/10.12974/2311-8717.2025.13.10